JOM
https://doi.org/10.1007/s11837-024-06771-4

Plasma/Ozone Induced PolyNaSS Graft-Polymerization onto PEEK Biomaterial for Bio-integrated Orthopedic Implants

CHANDRIMA KARTHIK,[1] RENJITH RAJAN PILLAI,[1] GERARDO HERNANDEZ MORENO,[1] PRABAHA SIKDER,[2] NAMASIVAYAM AMBALAVANAN,[3] and VINOY THOMAS [1,4]

1.—Department of Mechanical and Materials Engineering, University of Alabama at Birmingham, Birmingham, AL 35294, USA. 2.—Mechanical Engineering Department, Clevland State University, Clevland, OH 44115, USA. 3.—Department of Pediatrics, University of Alabama at Birmingham, Birmingham, AL 35233, USA. 4.—e-mail: vthomas@uab.edu

Owing to its superior bulk mechanical properties, poly (ether ether ketone) (PEEK) has gained popularity over the past 15 years as a metal substitute in biomedical implants. Low surface energy is a fundamental issue with PEEK implants. This low surface energy caused by a moderately hydrophobic surface may be able to inhibit cellular adherence and result in the development of an inflammatory response, which may result in cell necrosis and apoptosis. In this work, plasma and ozone treatments have been utilized to surface activate PEEK and graft ionic bioactive polymer polyNaSS (poly (sodium styrene sulfonate)) successfully on the surface to promote cellular attachment and biomineralization. The main goal of our research has been to find a stable green process for surface modification of PEEK by plasma/ozone approaches to increase PolyNaSS grafting efficiency and biomineralization. To further the field of bioactive orthopedic and dental implant technology, this research attempts to address a significant constraint of PEEK implants while preserving their favorable mechanical properties.

INTRODUCTION

The number of musculoskeletal pathologies, including fractures, low back pain, scoliosis, osteoporosis, bone infections, oral and maxillofacial pathologies, and rheumatic diseases such as osteoarthritis, is rapidly rising because of the aging global population and longer life expectancies.[1] Orthopedic implants are primarily used to support damaged tissue mechanically and structurally, integrate with the tissue, and deliver biological cues that aid in healing. Implant materials must be non-immunogenic, biocompatible, and able to properly integrate with the host tissue. Metal implants are the mainstay of modern surgical techniques for treating fractures and joint arthroplasties.[2] Nevertheless, implant motion, inflammation, bone resorption, and osteolysis brought on by implant wear, loosening, and incorrect loading may contribute to implant failure.[3,4] Before choosing metal-based implants, one must weigh their serious drawbacks against their benefits. Successful procedures can come with some serious drawbacks. Metal hypersensitivity can cause a variety of negative side effects, such as persistent discomfort and chronic inflammation. Depression, fibromyalgia, and chronic fatigue may be noted with metal hypersensitivity.[5,6] These negative consequences are typically mediated by implanted material degradation products, which are mainly produced by wear and corrosion. A variety of forms, including free metallic ions, colloidal complexes, inorganic metal salts or oxides, organic forms like hemosiderin, wear particles, etc., are some of the identified degradation products.[7]

Poly (ether ether ketone) PEEK, a partly crystalline polymer that has been extensively used in industry, has gradually made its way into the field of orthopedic/dental implants. It was approved as an implant material for orthopedic/trauma medicine by

(Received April 7, 2024; accepted July 11, 2024)

Published online: 16 August 2024

the Food and Drug Administration initially and later in neurosurgery.[10] PEEK has stable chemical and physical properties and a high elastic modulus (8.3 G Pa), closer to that of typical human bone (17.7 G Pa) than metal alloy implants (116 G Pa).[11,12] However, low surface energy is a major issue for PEEK for cellular adhesion and growth. Protein adsorption efficiency on the implant surface is influenced by surface chemistry, charge, wettability, and structure.[13,14] Using low-temperature plasma approaches, we can improve the surface energy of the implant material without affecting its bulk mechanical properties.[15,16] According to earlier research, polymers or copolymers containing anionic groups like phosphonates, carboxylates, and sulfonates can promote cellular attachment and differentiation. These ionic groups can act as active sites that can interact with extracellular proteins involved in cell adhesion/response, such as vitronectin or fibronectin.

In this work, we reported low-temperature air plasma to graft polyNaSS on the surface of PEEK by using a combined ozone irradiation and air plasma treatment to improve the surface energy of PEEK material before the grafting process. The degree of surface modifications can be effectively controlled with UV-ozone and air plasma treatments by adjusting variables such as exposure time, intensity, and source distance. The hydroperoxide groups formed on the surface were cleaved using argon plasma, producing radicals to initiate the polymerization process.[17] After samples had been immersed in NaSS solution, air plasma treatment was employed to complete the polymerization process. Normal and temperature-assisted (50°C) NaSS infiltration techniques were conducted to determine the efficacy of this integrated grafting technique. Samples were characterized and examined using a variety of methods, such as water contact angle (WCA) measurements, optical photo-thermal infrared spectroscopy (O-PTIR), scanning electron microscopy (SEM), x-ray photoelectron spectroscopy (XPS), atomic force microscopy (AFM), and MTT (3-(4,5-dimethylthiazol-2-yl)− 2,5-diphenyl-2H-tetrazolium bromide) assay, to demonstrate the effectiveness of our research.

MATERIALS AND METHODS

Materials

PEEK polymer sheets (purchased from K-mac Plastics), sodium styrene sulfonate (NaSS; purchased from Fischer, catalog no. 041690.30), ethanol (purchased from Fisher Scientific CAS: 64-17-5), water (purchased from Fisher, CAS: 7732185), toluidine blue-O (purchased from ACROS organics, CAS: 92319), MG-63 osteoblastic model cell line (from ATCC), MTT assay kit (Thermo Fisher CyQUANT MTT cell proliferation assay kit, catalog no. V13154), MEM 1x media (Minimum Essential Medium Eagle with Earle's salt without L-glutamine and phenol red purchased from Corning, reference number 17-305-CV), FBS (fetal bovine serum purchased from Corning, reference no. 35-015-CV), L-glutamine (purchased from Corning, reference no. 25-005-CI), antibiotic and antimycotic solution 100x (purchased from Corning, reference no. 30-004-CI), 0.25% trypsin (purchased from Corning, reference no. 25-053-CI), sodium chloride (NaCl; purchased from Arcos Organics), sodium bicarbonate ($NaHCO_3$; purchased from Arcos Organics), potassium chloride (KCl; purchased from Sigma-Aldrich), potassium phosphate dibasic trihydrate ($K_2HPO_4.3H_2O$; purchased from Arcos Organics), magnesium chloride hexahydrate ($MgCl_2.6H_2O$; purchased from Fisher Scientific), hydrochloric acid (HCl; purchased from Fisher Chemical, CAS: 7647010), calcium chloride ($CaCl_2$; purchased from Alfa Aesar), sodium sulfate (Na_2SO_4; purchased from Arcos Organics), and Tris (hydroxymethyl) aminomethane (Tris; purchased from Alfa Aesar).

Methods

Recrystallization of NaSS Monomer

Twenty grams of NaSS monomer was purified by recrystallization in 100 mL 90:10 v/v ethanol:water mixture before being used in the grafting process. After recrystallization, NaSS was dried overnight at 40°C and then stored at 4°C.[18]

Surface Activation of PEEK Polymer

PEEK samples were cut into 5-mm-diameter discs. PEEK discs were sonicated using 70% ethanol for 5 min. Two surface activation methods, UV-ozone (UVO), and atmospheric air plasma (AP) treatments were performed to determine the best approach for modifying the PEEK surface. Samples were treated for 30 min in a UVO system (NOVA SCAN PSD series digital UV Ozone system) and AP system (GLOW RESEARCH atmospheric air plasma system with an airflow 35 cc/min) separately to create the peroxide (-O-O-H) groups on the surface of PEEK materials.[19,20] After the peroxide formation on the surface, samples were irradiated with argon plasma using a glow plasma system for 10 min with 35 cc/min argon flow to cleave the peroxide bond and produce an oxide surface for aiding graft polymerization.

NaSS Infiltration

Surface-activated PEEK materials with oxide groups on the surface were immersed in 1 molar solution of aqueous NaSS monomer in two different conditions.

I. Temperature-assisted infiltration: UVO-treated samples and AP-treated samples with oxide surface were soaked in 1 molar NaSS solution for 24 h at 50°C.

II. Normal infiltration: UVO-treated samples and AP-treated samples with oxide surface were soaked in 1 molar NaSS solution for 24 h at room temperature.

After NaSS infiltration, UVO-temperature (UVO-T), UVO-normal (UVO-N), AP- temperature (AP-T), and AP-normal (AP-N) samples were collected for plasma-assisted grafting.

Graft Polymerization of NaSS

All four sets of samples were air plasma treated for 30 min in a glow discharge air plasma system with 40 cc/min airflow. After polymerization, the grafted surfaces were stirred for 30 min with de-ionized water and vacuum-dried for 24 h to remove the un-grafted monomer on the surface.

Surface Characterization

The efficiency of plasma-assisted grafting of polyNaSS was confirmed using water contact angle (WCA) measurements, toluidine blue-o (TBO) colorimetric assay, AFM roughness analysis, and XPS. The cytocompatibility of the material was determined by MTT assay. The samples were tested for biomineralization, and the surface were analyzed using SEM imaging.

Contact Angle Measurements

The wettability of the treated-PEEK and untreated samples was measured using a static solvent contact angle measuring system using water as solvent. Three samples were used in each group, and ten measurements were taken from each sample. A water droplet was suspended from the tip of a microliter syringe and placed on the surface of the sample. The images of the water droplet right after the contact were captured using a plugable digital viewer application connected to the camera. The image analysis was completed using ImageJ software. Ten measurements were taken for each sample, and the average value was reported with standard deviation.

TBO Colorimetric Assay and O-PTIR Study

To determine the efficiency of polyNaSS grafting, a toluidine blue colorimetric assay was conducted. Treated and untreated PEEK materials were immersed in 0.1 molar TBO solution in de-ionized water for 6 h at room temperature. After that, the samples were removed and completely washed using sodium hydroxide solution (pH 9). Any non-complexed molecules attached to the surface were completely washed off. This cationic molecule interacts with negatively charged groups through electrostatic interactions.[21] Using an O-PTIR (mIRage IR microscope, Photothermal Spectroscopy Corp., USA) imaging facility, TBO distribution on the PEEK surface was imaged. The samples were illuminated with a tuneable pulsed mid-IR quantum cascade laser (QCL: 1150 cm^{-1} and 1 to 40 mV voltage) to obtain the TBO distribution on the PEEK surface.

XPS Analysis

XPS analyses were conducted using a PHI 5000 Versa probe imaging XPS equipped with a focused, monochromatic Al Kα radiation source (E = 1486.6 eV) x-ray beam with an electron beam power of 25 W and 100 μm spot size. To neutralize any charge in the spectra, an argon ion cannon was used to regulate the charge. For the analysis, Multipakv9.0 programming was used. Triplicates per group were analyzed to assure the reproducibility of the treatment.

AFM Surface Roughness Analysis

For sample surface roughness analysis and imaging, ezAFM compact AFM (NanoMagnetics Instruments) was used along with an ezAFN/ ezSTM controller and vibration isolator (Minus K Technology). Analysis was done in the 20 $\times$ 20 μm scan range (0 to 1.5 V) in tapping mode (three 20 μm $\times$ 20 μm areas scanned per sample).

Biomineralization Studies

Simulated body fluid (SBF) for the biomineralization studies was prepared as per previously reported work from our group.[22] The following reagents were added to 500 mL deionized (DI) water and thoroughly mixed to prepare a 500 mL SBF solution: 5.997 g NaCl, 0.263 g $NaHCO_3$, 0.168 g KCl, 0.172 g K_2HPO_4 $3H_2O$, 0.0229 g $MgCl_2$ $6H_2O$, 30 mL HCl 1 M solution, 0.208 g $CaCl_2$, 0.0503 g Na_2SO_4, and 4.543 g Tris. The HCl solution was used to buffer the solution until its pH was 7.40 $\pm$ 0.02. Samples (n = 5 per treatment group) were submerged individually in 3 ml SBF solutions for 10 and 20 days. The samples were incubated at 37 $\pm$ 1°C in the SBF solution. Every 72 h, the SBF solution was replaced to maintain the ion concentration. Samples after biomineralization were washed with de-ionized water and dried under vacuum. To understand the rate of biomineralization, samples were imaged using a FE-SEM (FEI Hillsboro) scanning electron microscope at 10 kV. Samples were sputter coated using an Au-Pd chamber for 1 min before imaging.

Cell Culture Studies and MTT Assay

The cytocompatibility of the samples was evaluated using MTT assay. M6-63 osteoblast-like cell line from ATCC was used to perform the assay. Cells were cultured in MEM medium with 10% FBS, 1% glutamine, and 1% antibiotic and antimycotic solution in a tissue culture flask. Cells were harvested at 80-90% confluence by treatment with 0.25% trypsin. The assay was performed using the

"CyQUANT MTT cell proliferation assay kit" (n = 5 per treatment group). Cells were plated and incubated along with PEEK materials in a 96-well plate. Cell viability assay was performed as per the protocol provided by the manufacturer (publication no. MAN0019028). An automated cell counter (Bio-Rad TC-20) was used to count the cells. In a 96-well plate, cells were seeded onto the samples at a density of 30,000 cells/100 μL for each well. Following the manufacturer's instructions, the plate was analyzed at an absorbance of 570 nm after 72 h of incubation using a microplate spectrophotometer (Benchmark plus, Bio-Rad). Statistical analysis (one-way ANOVA) was conducted using GraphPad Prism.

RESULTS AND DISCUSSION

Graft Polymerization of NaSS Monomer in the PEEK Surface

During surface activation, the PEEK surface was subjected to the bombardment of ionized air under vacuum. The surface chemical reactions induced by the ionized gas modified the surface energy of the PEEK. The high-energy surface groups are typically formed because of the interactions between the native polymer surface groups and reactive plasma species. This increased surface energy was the reason behind the hydrophilicity of the material. The process of plasma treatment entails subjecting the material to a partially ionized gas made up of neutral particles, ions, and electrons. The ionized gas particles cause chemical reactions on the surface of materials, particularly polymers when they are subjected to plasma. These reactions may result in the creation of high-energy surface groups like carboxyl, carbonyl, or hydroxyl groups, which raise the surface energy of the material and hydrophilicity.[23–25] UV-ozone treatment modifies a material's surface properties by combining ozone (O3) with ultraviolet (UV) light. Ozone is created by the UV radiation from atmospheric oxygen, and the ozone then interacts with the surface of the substance. Usually, this reaction results in the creation of functional groups that include oxygen, much like those produced by plasma treatment, and which make the material more hydrophilic. The improved surface energy and hydrophilicity of the implant surface leads to better wetting, which facilitates stronger and more uniform cell adhesion. Hydrophobic recovery, in which the treated surface eventually reverts to its initial, less hydrophilic form, was one of the difficulties associated with these treatments, though. This recovery is explained by either low-energy molecules migrating from the bulk of the material to the surface or the reorientation of the surface molecules. A calculated tactic to address the issue of hydrophobic recovery in materials treated with plasma or UV-ozone to enhance their hydrophilicity was grafting with hydrophilic polymers. After air plasma and UV-ozone treatments, the hydroperoxides formed on the surface were cleaved by argon plasma to create oxide groups. After argon plasma treatment, the samples were immersed in 1 molar NaSS monomer solution to ensure the complete infiltration of monomer into the polymeric substrate.[18,26] Higher temperatures enable NaSS molecules to possess more kinetic energy and facilitate more penetration into the PEEK surface. The chosen temperature should be high enough to enhance diffusion and reaction kinetics without compromising the integrity of the materials involved. During infiltration, the radicals on the surface initiate the graft polymerization process (grafting from) and air plasma treatment after the infiltration (grafting to) completes the graft polymerization process. To optimize the efficiency of polyNaSS grafting and finalize the mechanism of grafting, a toluidine blue colorimetric assay was performed. This whole process was a combined method of grafting-from and grafting-to approaches to improve the graft polymerization of poly NaSS in the PEEK surface.

Contact Angle Measurements

Surface wettability is a crucial factor that determines cell adhesion.[27] The wettability was analyzed from the water contact angle measurements as shown in Fig. 1. The contact angle of the untreated PEEK sample was 76 ± 0.17^0, indicating the hydrophobicity of the sample, and the treated samples lie in the hydrophilic range. The plasma surface activation and polymerization on the surface of the PEEK material lead to the maximum grafting of hydrophilic polyNaSS. Samples after the graft polymerization were washed and dried under a vacuum to ensure the complete removal of ungrafted monomeric groups from the surface.[28,29] Samples were first rinsed three times with deionized water for 5 min each. The samples were then vacuum-dried in a vacuum desiccator at room temperature (23 $\pm$ 2°C). The UV-ozone pretreated sample UVO-T showed higher hydrophilicity compared to the other treated samples (Fig. 1). This may be due to the increased radical formation on the sample after surface treatments. Temperature-assisted infiltration can increase the energy and improve the grafting-from process. This may be the reason behind the improved hydrophilicity of temperature-assisted infiltrated samples compared to the normal samples. Cell attachment and proliferation are better suited for hydrophilic surfaces. Hydrophilic surfaces promote cell adhesion more than hydrophobic ones, especially for cells involved in tissue regeneration. In addition to facilitating cell proliferation and tissue regeneration, this encourages improved implant integration with adjacent tissues.[30,31] Hence, the contact angle data can be considered a key parameter in optimizing the hydrophilicity of the implant material.

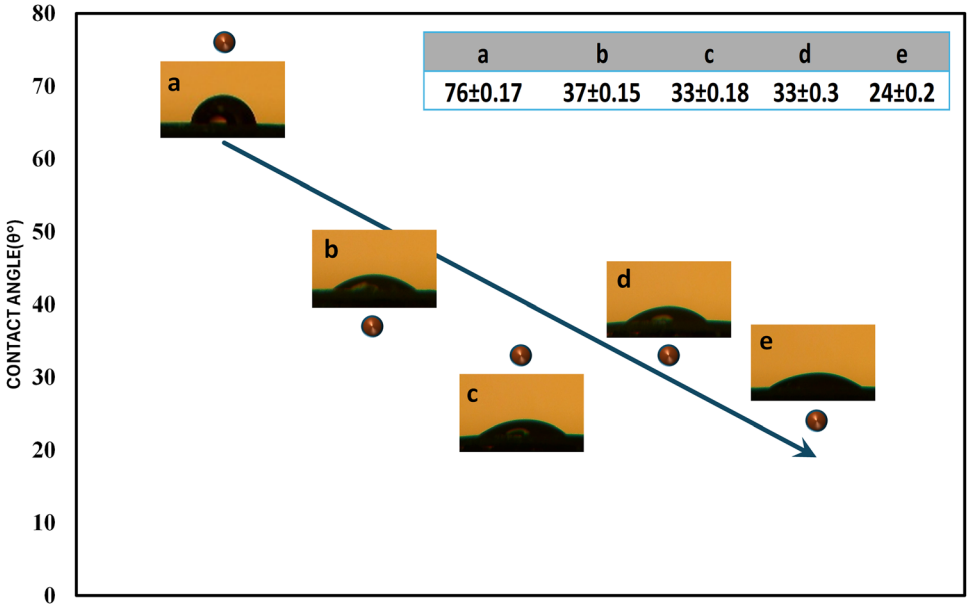

Fig. 1. Water contact angle of PEEK samples: **a** untreated PEEK, **b** AP-N, **c** AP-T, **d** UVO-N, **e** UVO-T.

TBO Colorimetric Assay and O-PTIR

Toluidine blue is a cationic dye that is frequently used in cytology and histology to stain nucleic acids, especially DNA and RNA. With a few exceptions owing to the polymer composition, the process for staining polymeric materials like polyNaSS can be comparable to that for biological specimens. Toluidine blue has a cationic group containing thiazine metachromatic dye. This cationic group is the quaternary amine group, which is situated on the phenothiazine ring structure. The thiazine ring is made up of nitrogen atoms with three connected hydrogens, whereas the quaternary amine group, which carries the positive charge, is made up of nitrogen atoms with four hydrogens. The cationic features found in toluidine blue are induced by this positively charged group. There are negatively charged sulfonate groups in polyNaSS. Electrostatic interactions cause the cationic dye molecules in an aqueous solution to be drawn to the negatively charged polyNaSS polymer chains. Toluidine blue may establish ionic connections with the sulfonate groups in the polymer after being adsorbed onto the scaffold surface. The dye-polymer bond is stabilized by this interaction. The molecules of toluidine blue that have adhered to the surface aid in the polymer staining. Once the sample has been stained, it is usually washed to get rid of any dye molecules that have not attached to the polymer surface. Here, toluidine blue adsorption on the PEEK surface was determined by O-PTIR imaging. Using an infrared absorption property-based approach, with sensitivity down to the nanoscale, O-PTIR offers the advantage of high spatial resolution images. The alterations brought on by the photothermal heating are tracked using an optical detecting device with high sensitivity. Usually, a microscope objective is used in this detection system to direct the infrared beam onto the sample and gather the signal that is produced. A spatial map of infrared absorption properties can be produced by moving the infrared beam across the sample and measuring the signal that results at each location. The distribution and concentration of IR-absorbing moieties within the sample are shown on this map (Fig. 2).[32]

According to the previous literature, the most important peak to consider when examining the TBO FTIR spectrum for sulfate staining purposes is the peak connected to the quaternary ammonium group ($N(CH_3)^{3+}$). Usually, this peak comes between 1100 and 1200 cm^{-1}. The complete FTIR spectrum of TBO can be found at spectrabase.com/Wiley Spectra base (Hoboken, NJ, USA).[33] This peak is significant because it symbolizes the distinctive functional group in toluidine blue O that interacts with sulfate ions during the staining procedure. The dye molecules bind to sulfate-rich structures because of electrostatic interactions between the positively charged quaternary ammonium groups in TBO and the negatively charged sulfate ions.[34,35] Considering this, chemical mapping was carried out at 1150 cm^{-1} to get the most accurate information, and imaging was carried out at 40 mV power in a 40 × 40 μm area. O-PTIR images of the TBO dye adsorbed samples are given in Fig. 2. A higher concentration of TBO is marked with red, and the color profile changes depending on the concentration of TBO adsorbed. In the control sample, a minor amount of red color was visible, maybe because of the presence of dye entrapped in the minor scratches of the polymer surface. The PEEK sheets used in this experiment are calendared samples with micro-tears on the surface due to mechanical

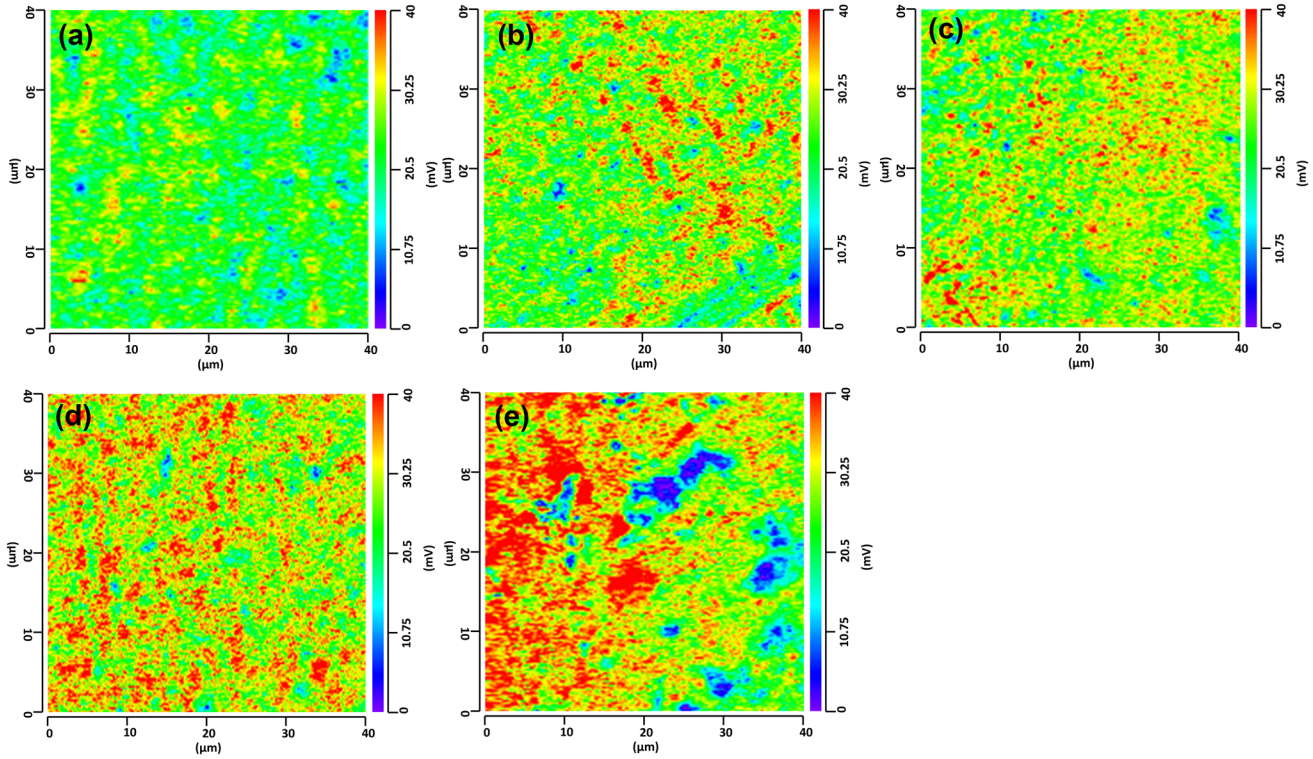

Fig. 2. O-PTIR images of the TBO-stained PolyNaSS-grafted PEEK samples: **a** untreated PEEK, **b** AP-N, **c** AP-T, **d** UVO-N, **e** UVO-T at 1150 cm^{-1}.

processing. The air plasma pretreated samples after normal and temperature-assisted NaSS infiltration showed better TBO adsorption compared to the control. There were areas with a higher concentration of dye indicating the presence of more sulfate groups on the surface of the PEEK. A considerable increase in dye adsorption can be seen in ozone-pretreated samples, especially ozone-pretreated temperature-assisted NaSS-infiltrated samples. These images confirm the efficiency of grafting and the influence of temperature-assisted NaSS infiltration. Even though NaSS monomers tend to recrystallize at higher temperatures, a small temperature change accelerated the grafting efficiency of the entire process. Air plasma-pretreated normal samples and ozone-pretreated normal samples have less adsorption of TBO compared to the temperature samples, indicating the effect of temperature to initiate the grafting-from process. After infiltration, plasma-assisted grafting-to process increases the yield of grafting by giving more energy to polymerize the ungrafted monomeric groups.

XPS Analysis

XPS has been used to further examine the differences in the surface characteristics of the PolyNaSS-grafted PEEK samples. The percentage contributions of carbon, oxygen, sulfur, and sodium on treated and untreated surfaces are shown in Table 1 based on the survey scan of the XPS spectra. The carbon content of treated samples was less compared to the untreated PEEK samples. While grafting, polyNaSS adds more non-carbon atoms to the PEEK surface. The overall percentage of carbon in the sample falls compared to other elements because of the grafting process. These additional atoms, especially sodium and sulfur, raise the overall atomic proportion of non-carbon elements, which lowers the relative carbon content.[36] Also, a slight trend of increased atomic percentage of oxygen in treated samples compared to untreated samples can also be seen in this survey scan result.

The atomic percentages of sulfur in air plasma pretreated normal and temperature-assisted NaSS infiltrated samples are 3.7% and 5.7%, respectively, showing the higher grafting in temperature-assisted monomer infiltrated sample. The atomic percentage of Na also has a similar trend in these samples. However, in the AP-N sample, the amount of sulfur and sodium grafted are almost similar. The atomic percentages of sulfur in UVO-N and UVO-T samples are 6.4 and 7.7, respectively. The atomic percentages of Na in AP-N and UVO-N are comparable but the percentage of sulfur was high in UVO-N. The additional presence of Na1s of around 1071 eV (together with its corresponding Auger peak around 495 eV) and S2p of around 168 eV (together with the S2s peak at around 230 eV) in each survey spectrum after the polyNaSS grafting under various conditions indicates the successful grafting of polyNaSS onto these PEEK surface. A similar trend in grafting can be seen compared to

Table 1. Elemental surface chemical analysis data from XPS

Sample	C1s (%)	O1s (%)	S2p (%)	Na1s (%)
Untreated PEEK	68.1 ± 0.2	23.4 ± 1.7		
AP-N	67.9 ± 1.5	23.6 ± 0.7	3.7 ± 0.2	3.5 ± 0.11
AP-T	62.4 ± 0.9	25.1 ± 0.31	5.7 ± 0.13	4.9 ± 0.21
UVO-N	60.4 ± 1.83	27.4 ± 0.42	6.4 ± 0.24	3.5 ± 0.1
UVO-T	58.9 ± 0.89	28.0 ± 0.37	7.7 ± 0.13	4.1 ± 0.2

the TBO colorimetric analysis. UVO-N and UVO-T samples show the highest yield. The efficiency of temperature-assisted Nass infiltration and synergistic effect of grafting-from and grafting-to processes are confirmed by the XPS data.

AFM Surface Roughness Analysis

The surface qualities of materials, especially their roughness, can be changed by the plasma treatment. Particle etching, surface activation, and deposition are a few of the ways via which plasma treatment of materials like PEEK can create variations in surface roughness. By subjecting PEEK to a barrage of high-energy ions, plasma can etch its surface. Depending on the nature of the material and plasma temperatures, this etching process can remove material from the surface, leaving it either rougher or smoother. For example, setting the plasma settings to high energy can result in greater material removal (etching) and raise the surface roughness. On the other hand, better-controlled circumstances can lead to a smoother surface. Plasma surface activation can change the surface chemistry, becoming more hydrophilic or reactive. Surface roughness can change as a result of defects or functional groups forming because they can create new surface features or affect surface energy.[37] We were aiming to activate the surface and utilize this increased surface energy to enhance the hydrophilicity and grafting. It is possible to regulate the impact of plasma treatments on surface roughness by varying several factors, including pressure, gas composition, treatment duration, and plasma power. It is feasible to modify the surface roughness of PEEK to satisfy needs for various applications by adjusting these parameters. Optimizing the roughness of the material without compromising the hydrophilicity and grafting efficiency along with cytocompatibility was the most challenging step in the process optimization part.[38] The ability of cells to attach to the substrate might be impacted by surface roughness. Generally, moderately rough surfaces tend to encourage cell attachment more than those that are exceedingly smooth or rough. This is because moderate roughness delivers mechanical cues that resemble the extracellular matrix found in nature as well as increased surface area for cell attachment. However, because of their higher physical barriers or smaller contact areas, extremely rough surfaces may prevent cell attachment. Surface roughness can affect the cytoskeletal structure, spreading, and shape of cells. On moderately rough surfaces, cells tend to proliferate more widely, improving cell viability and cell-substrate interactions.[39] Surface roughness can affect the cellular proliferation rates. In contrast, extremely rough or uneven surfaces may hinder cell proliferation because of increased stress or decreased cell-substrate interactions. Moderate surface roughness may promote cell proliferation by offering mechanical cues for cell division and anchoring locations. Similarly, a rough surface might offer more grafting sites, increasing the surface area that is accessible for the reaction to take place. On the other hand, extremely rough surfaces can prevent uniform grafting and result in inadequate coverage.[40,41] On the other hand, the grafting procedure can change the polymer surface roughness. For example, depending on the process and conditions of the grafting reaction, it may fill in surface imperfections or create new ones. Here, we have performed both plasma surface activation and grafting. So, the change in roughness plays a crucial role in determining the efficiency of the biomaterial. Using a compact AFM, the surface morphology of the samples was analyzed. Surface topology images, 3D images, and roughness values were collected to make sure the surface roughness of the material was suitable for the application. AFM analysis was performed in tapping mode along with a vibration isolator. A 20 × 20 μm sample area was considered for analysis, and the roughness data are tabulated in Table 2.

Surface roughness average (Ra) values were completely comparable with the XPS and colorimetric analysis. Ra values can give an in-depth understanding of the properties of surface texture and have good correlations with other surface roughness metrics. Ra was hence a useful metric in our proposed work to characterize surface roughness. The UVO-T samples had the highest surface roughness of 28.24 nm. The surface roughness of air plasma pretreated samples was similar, and a slight increase could be seen in temperature-assisted infiltrated samples. According to these results, the pretreatments increased the roughness of the material, which decreased after the grafting. The roughness created after the pretreatment may be the

reaction site for grafting. However, after grafting, because of the presence of grafted polyNaSS, the surface of the material decreased. According to the previous XPS, contact angle, and TBO analyses, the rate of grafting was higher in temperature-infiltrated samples, especially the UVO-T sample. A higher grafting rate can be the reason for the increased surface roughness of those samples. Accumulation of polyNaSS on the surface of the PEEK resulted in higher surface roughness values in the treated samples. The maximum surface amplitude of the control sample was 241.24 nm. Treated samples excluding AP-N have higher maximum amplitude compared to the control. The UVO-T sample has a very high amplitude similar to the roughness values. This may be due to the higher grafting rate in that sample. Topological imaging of the treated and untreated samples helped confirm the absence of any larger polyNaSS entities on the surface. Figure 3 represents the topological and 3D images of the samples. The surface topology of all the treated samples was found to be similar to the untreated PEEK sample. The absence of macro-micro entities on the surface proves the efficiency of grafting. The presence of physiosorbed moieties can falsify the data, and these moieties can be easily removed from the surface.

Biomineralization Studies

The process of osseointegration, which refers to the direct anatomical and functional bond between the surface of an artificial implant supporting load and living bone, is essential to the long-term viability of implants. PEEK becomes more hydrophilic after being treated with plasma, which changes its surface energy. This improved wettability promotes protein adsorption, which is necessary for cell attachment and the subsequent integration of the bone. The PEEK surface may undergo micro-

Table 2. AFM surface Ra measurements and maximum amplitude measurements of untreated and treated PEEK samples

Sample	Ra values (nm)	Maximum amplitude (nm)
Untreated PEEK	23.96 ± 1.84	241.24
AP-N	21.56 ± 0.94	233.52
AP-T	21.96 ± 0.71	280. 53
UVO-N	24.95 ± 0.26	279. 99
UVO-T	28.24 ± 0.57	287.98

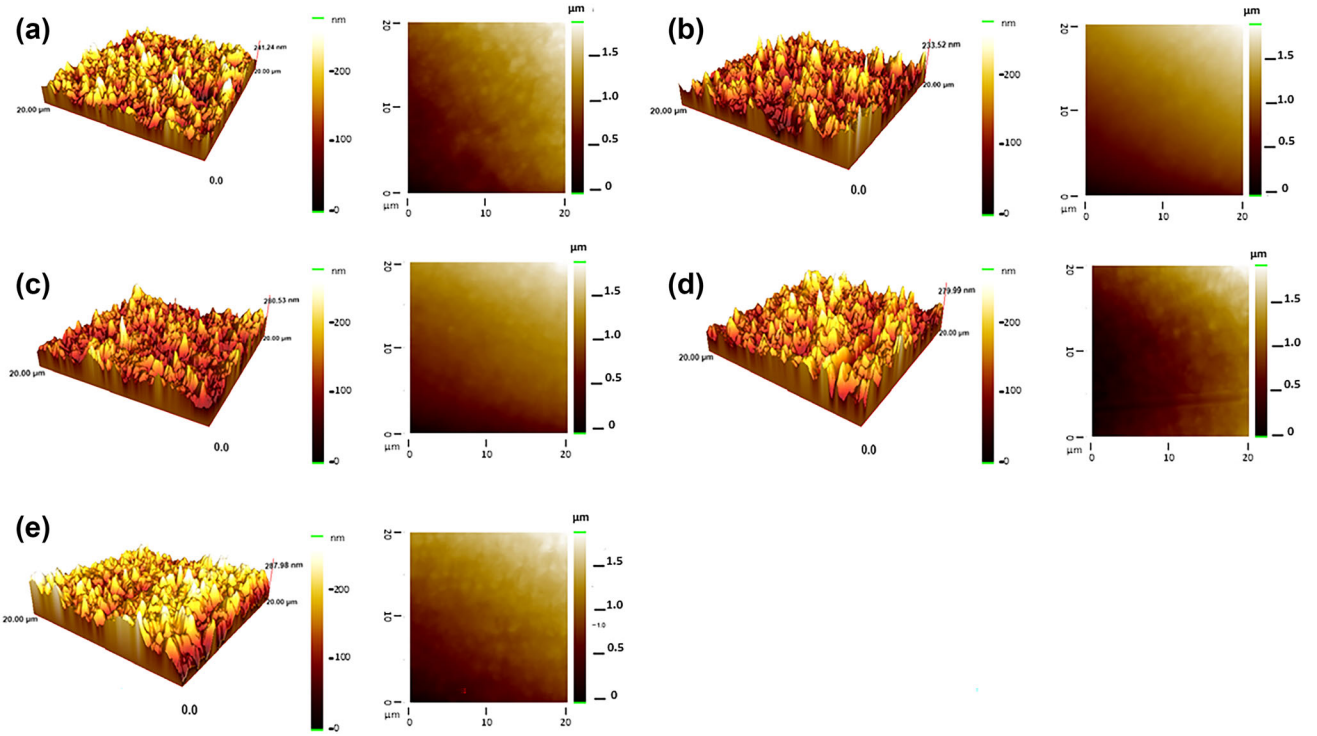

Fig. 3. Tapping mode topological and 3D AFM images of samples: **a** untreated PEEK, **b** AP-N, **c** AP-T, **d** UVO-N, **e** UVO-T.

and nano-scale topographical alterations as a result of plasma treatments. By imitating the natural architecture of bone, these modifications can encourage osteoblast adhesion and proliferation as well as bone ingrowth. PolyNaSS is a sulfonated polymer that has been shown to have biological effects.[42,43] The introduction of sulfonic acid groups to the surface of PEEK by grafting boosts the hydrophilicity and provides functional groups that could potentially improve bone cell adhesion and proliferation, ultimately facilitating osseointegration. Calcium and phosphate ions, which are necessary for bone mineralization, can be drawn to the sulfonic acid groups that NaSS introduces. This can promote osseointegration by causing a calcium phosphate layer to grow on the implant surface that resembles bone. Prior studies have shown that NaSS-modified implants can substantially enhance cell growth, proliferation, extracellular matrix secretion, calcification, alkaline phosphatase activity, and osteogenesis-related gene expression.[44]

The vacuum-dried biomineralized samples were imaged under SEM to understand the morphology of the nuclei formation and determine the efficiency of treated samples compared to the untreated PEEK. Ten days of biomineralized samples (Fig. 4) showed the initial nuclei formation phase of biomineralization. All the samples including the untreated PEEK started showing small nuclei on the surface after 10 days. The size of the nuclei in the control sample was very small compared to the treated samples. In air plasma surface-activated samples, more nuclei are visible in temperature-assisted NaSS-infiltrated samples. The calcium phosphate complexes (CaP) are maximumly deposited in UVO-N and UVO-T samples. In the UVO-T sample, a complete layer of deposition can be seen, which indicates the faster mineralization of the sample. The absence of tiny nuclei in the UVO-T sample showed the early growth phase of CaP complexes (Fig. 4F). All the other treated samples except UVO-T are still in nucleation. The CaP mineral crystals start to grow after nucleation. The crystals become larger as a result of this expansion, which usually entails the deposition of extra mineral ions onto the preexisting nucleus.

SEM analysis of samples after 20 days of biomineralization confirmed the osseointegration potential of polyNaSS-grafted samples (Fig. 5). After 20 days of biomineralization, the control sample showed the presence of an unstable CaP complex on the surface accumulated in the form of layers and peeling off from the surface as shown in Fig. 5d. All the treated samples are in the growth phase, but the presence of small nuclei in AP-N and UVO-N samples indicates the slower biomineralization process. AP-T and UVO-T samples are completely in growth. Large CaP agglomerated complexes are visible on the surface of AP-T and UVO-T samples indicating the higher osseointegration potential of temperature-

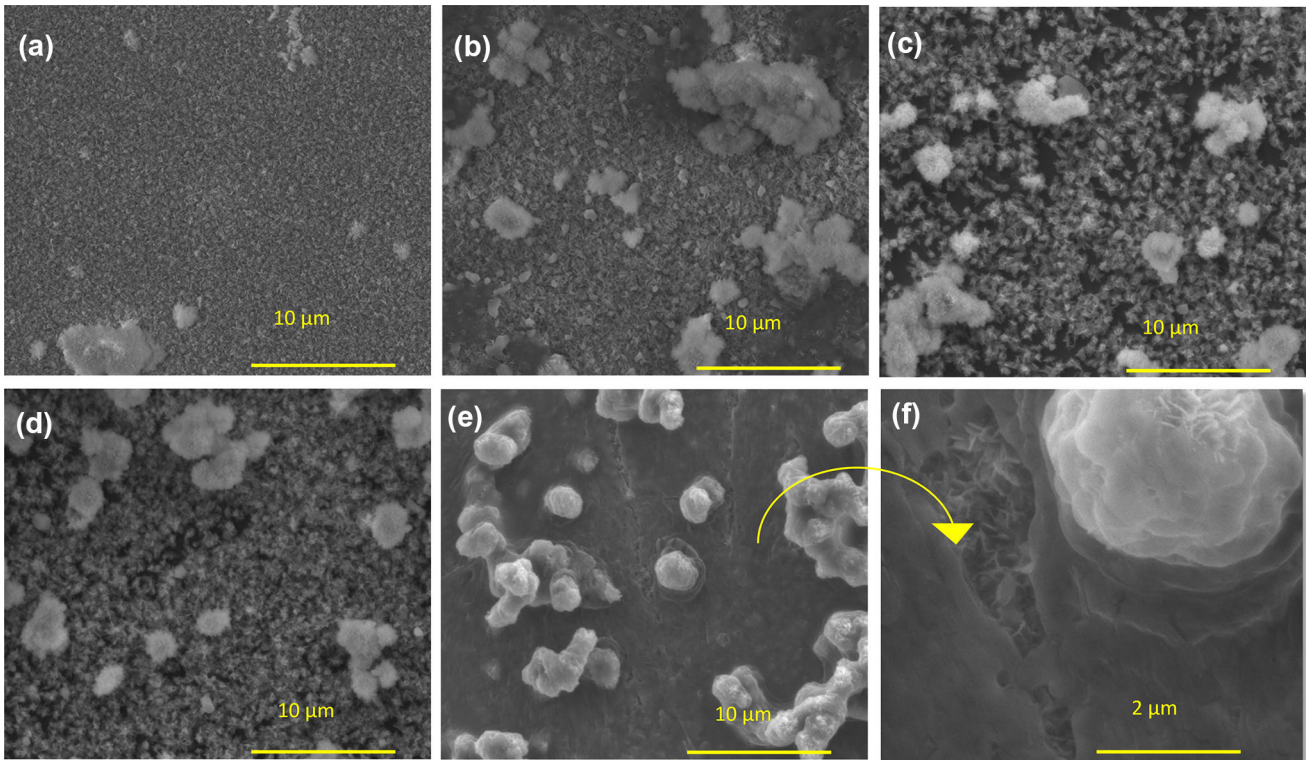

Fig. 4. SEM images of biomineralized samples: **a** untreated PEEK, **b** AP-N, **c** AP-T, **d** UVO-N, **e** UVO-T, **f** magnified image of the UVO-T sample showing CaP accelerated growth phase after 10 days. Images **a**, **b**, **c**, **d,** and **e** were collected at 5000 × magnification and image **f** at 30,000 × magnification.

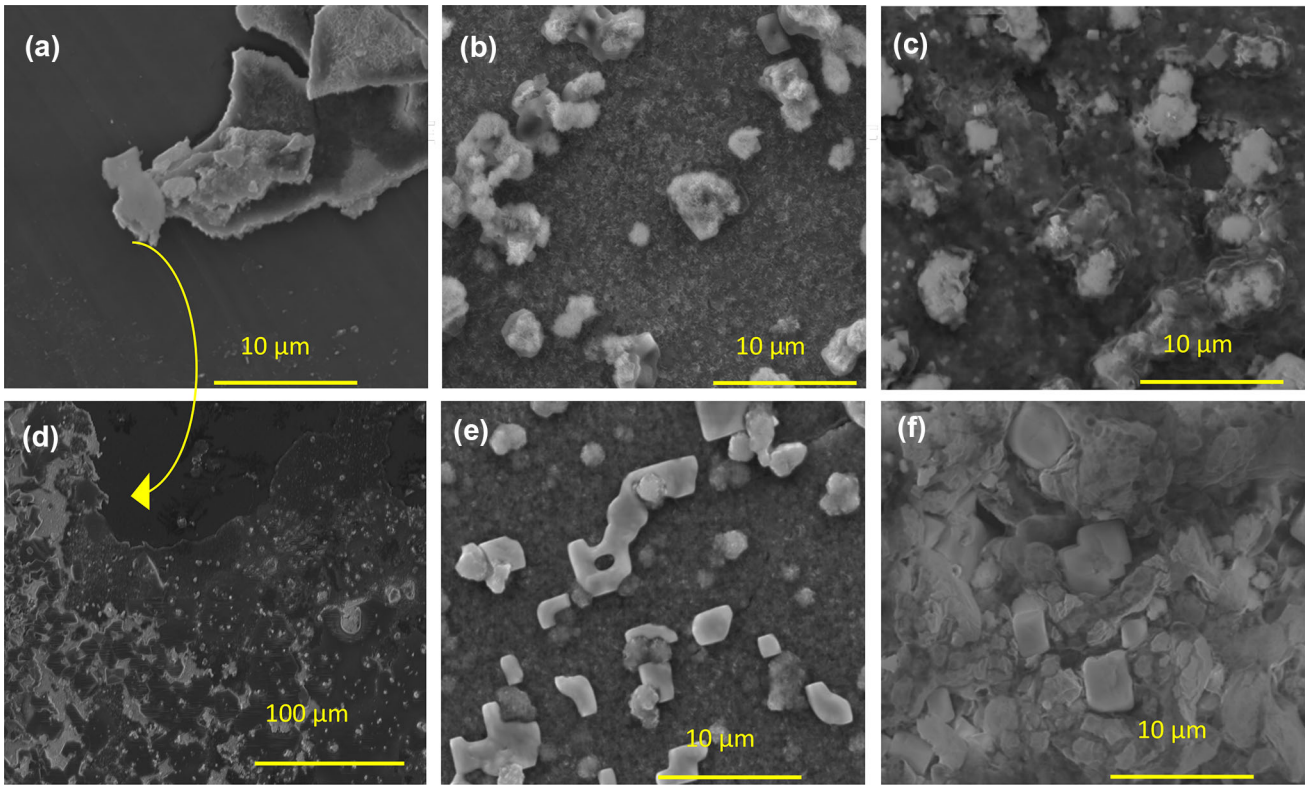

Fig. 5. SEM images of biomineralized samples: **a** untreated PEEK, **b** AP-N, **c** AP-T, **d** 500 × magnified image of untreated PEEK showing the peeling off of CaP complexes and visible polymer matrix, **e** UVO-N, and **f** UVO-T after 20 days. Images **a**, **b**, **c**, **e**, **f** were collected at 5000 × magnification and image **d** at 500 × magnification.

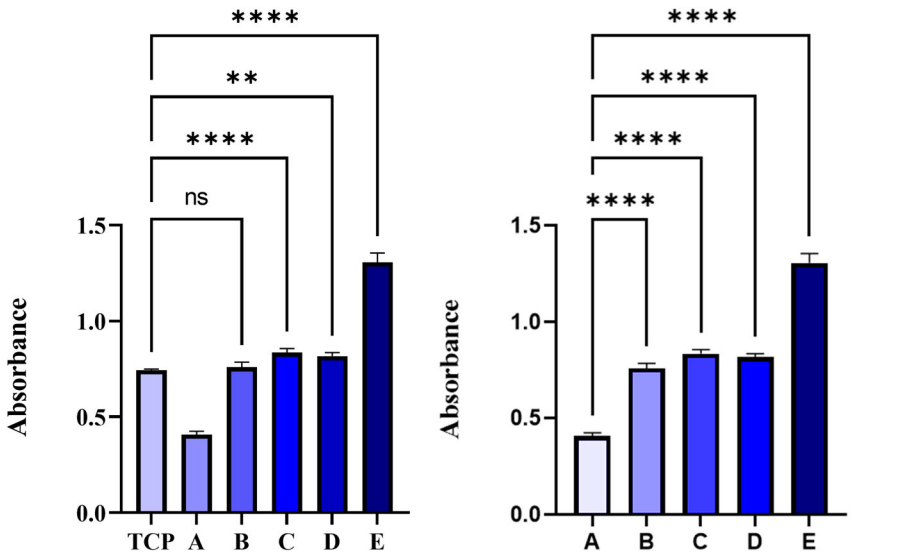

SAMPLE	ABSORBANCE
TCP	0.744±0.005
a	0.406±0.017
b	0.759±0.026
c	0.835±0.021
d	0.817±0.018
e	1.305±0.049

Fig. 6. Effect of treated and untreated PEEK scaffolds on cell viability. Absorbance values of TCP (tissue culture plated), **a** un-treated PEEK, **b** AP- N, **c** AP-T, **d** UV-N, and **e** UV-T samples after MTT assay. Assay was performed after 72 h of cell growth.

assisted infiltrated samples. UVO-T samples are very stable without any unstable nuclei on the surface has the highest osseointegration potential. The scattered salt-like entities on the UVO-N samples are an indication of unstable nuclei. Biomineralization studies also showed the combined potential of grafting-from and grafting-to methods in treated AP-T and UVO-T samples (Fig. 6).

MTT Cell Viability Assay

MG-63 cells are a type of human osteosarcoma cell line that bears many similarities to osteoblasts, the cells that build bones. These cells are frequently employed in in vitro investigations to assess the osteogenic potential and biocompatibility of biomaterials meant for use in bone implant applications. Through surface chemistry and topographical modifications, plasma treatments improve the osteogenic potential and bioactivity of the PEEK. The introduction of sulfate functional groups and development of a surface that is more conducive to cell contact enhance osteoblast function, resulting in higher mineral deposition, collagen production, and alkaline phosphatase activity. These outcomes suggest increased bone matrix production and osteogenic differentiation, both of which are necessary for implant stability and effective bone integration.

The MTT assay is a colorimetric method that evaluates cell viability by measuring the metabolic activity of cells. The MTT assay works based on the idea that only live cells capable of metabolic activity can change the yellow MTT (3-(4,5-dimethylthiazol-2-yl)−2,5-diphenyltetrazolium bromide) into purple formazan. The formazan crystals are dissolved after an incubation period, and a spectrophotometer was used to measure the absorbance of the solution. The absorbance value, which represents color intensity, is correlated with the quantity of metabolically active cells in the culture. Higher absorbance readings indicate a greater number of viable cells, and this association makes it possible to quantify cell viability. These MTT absorbance results revealed that, after 72 h of incubation, the cell survival rate in all the treated samples was high or similar compared to the TCP. The untreated PEEK showed a very poor cell viability rate.

The tissue culture plate-grown cells showed an absorbance rate of 0.744 AU. The cell viability of MG-63 cells plated in the untreated PEEK reduced to nearly half compared to the plated cells. The cytocompatibility of plated cells in the AP-N, AP-T, and UVO-N samples was 0.759, 0.835, and 0.817, respectively. All the treated samples were significant compared to the control. All the samples showed similar or improved cell viability results compared to the TCP. The detailed p values are mentioned in supplementary Fig. S-1 and Fig. S-2. The highest cell viability absorbance rate was observed in the UVO-T sample. All the temperature-infiltrated samples showed a significant increase in cell viability. The importance of temperature-assisted infiltration was reflected in these data. These outcomes were consistent with expectations based on data from biomineralization, colorimetric studies, XPS, and contact angle data. Cell adhesion, spreading, and matrix penetration take longer on scaffolds, particularly those with intricate architectures and high surface-to-volume ratios.[45] The polymer can be seeded and distributed more uniformly for 72 h, ensuring that the MTT experiment accurately reflects the viability of cells throughout the whole scaffold. The 72-h duration permits multiple rounds of cell division, thus offering a more thorough evaluation of both the viability and proliferation of cells in the scaffold environment.[46] Only moderately hydrophilic surfaces allow for optimal cell attachment. Cell attachment and spreading are either entirely inhibited or limited on very hydrophilic surfaces, particularly super-hydrophilic surfaces.[47] PolyNaSS grafting introduces sulfonate groups to the PEEK surface, potentially enhancing its biomineralization in vitro. These sulfonate groups could have favorable interactions with biological substances and cells, which improve the vitality and attachment of the cells.

CONCLUSION

The purpose of this study was to find a stable grafting method for PEEK implants using air plasma and UV-ozone treatments. An integrated grafting-from, grafting-to approach was employed in this research. The presence of oxide groups in the surface-activated PEEK triggered the grafting-from process and the presence of high energy electrons and ions in air plasma triggered the grafting-to process. When comparing the PolyNaSS-grafted PEEK to the untreated PEEK, we found a considerable decrease in WCA values, which suggests improved hydrophilicity and effective surface modification. The OPTIR data confirm the uniform distribution of the grafted polymer across the PEEK surface. The change in nanoscale features observed in the AFM results further supports the presence of the grafted PolyNaSS layer. The XPS data confirm the presence of sulfur and sodium in the treated samples. Based on the results, the rate of graft polymerization was high in the temperature-assisted monomer infiltrated samples compared to the room-temperature monomer infiltrated samples. The biomineralization and cell viability studies confirmed the potential of this engineered PEEK polymer to serve as an effective implant material.

In conclusion, the bioactive PEEK biomaterial grafted with polyNaSS may be considered for the upcoming generation of bioactive synthetic implants, given the outcomes of this work. To precisely capture the various application domains of these prospective scaffolds, additional research using alternative scaffold materials and monomer types has to be done. Future studies will involve grafting various functionalities on the surface of the 3D-printed implants using a plasma-assisted graft-polymerization approach and preclinical studies. It may be possible to improve bone-implant interactions by adding more functional groups (such as carboxylate or phosphonate moieties) to the NaSS monomer structure. To compare these grafted PEEK to commercial implants in terms of osseointegration and inflammatory response, long-term preclinical research in large animal models is essential.

SUPPLEMENTARY INFORMATION

The online version contains supplementary material available at https://doi.org/10.1007/s11837-024-06771-4.

ACKNOWLEDGEMENT

We acknowledge National Science Foundation funding support through NSF EPSCoR OIA-2148653 for "Future Technologies Enabled by Plasma Process." All opinions presented here are solely those of the authors and do not necessarily reflect the opinions of NSF, USA. Thanks are also due to Dr. Mark Banaszak Holl and Dr. Blessy Joseph for providing the O-PTIR and AFM facilities. We thank Brian Halloran from the Department of Paediatrics for providing the cell culture facility and Dhanisha Sulekha Suresh from the Department of Surgery for the statistical analysis.

CONFLICT OF INTEREST

The authors declare that they have no conflict of interest.

OPEN ACCESS

REFERENCES

1. R. Agarwal, and A.J. García, *Adv. Drug Deliv. Rev.* 94, 53 (2015).
2. C. N. Elias, J. H. C. Lima, R. Valiev, and M. A. Meyers, Biol. Mater. Sci. 1 (2008).
3. T.W. Bauer, and J. Schils, *Skeletal Radiol.* 28, 423 (1999).
4. D.S. Garbuz, B.A. Masri, and A.A. Czitrom, *Orthop. Clin. North Am.* 29, 199 (1998).
5. Z.W.W. Teo, and P.C. Schalock, *J. Investig. Allergol. Clin. Immunol.* 26, 279 (2016).
6. S. Pallickal Babu, S. Sam, B. Joseph, N. Kalarikkal, R. E.K., R. Nair, and S. Thomas, *Nanoscale Polymer Coatings for Biomedical Implants* (Elsevier Inc., 2023).
7. R.V. Badhe, O. Akinfosile, D. Bijukumar, M. Barba, and M.T. Mathew, *Toxicol. Lett.* 350, 213 (2021).
8. D.M.B. James, *Int. J. Res. Appl. Sci. Eng. Technol.* 8, 396 (2020).
9. M. Joseph, M.S.R. Pathiripparambath, V. Thomas, H. Tharayil, R.S. Jayasree, and L.V. Nair, *J. Mater. Chem. B* 12, 720 (2023).
10. N. Blanch-Martínez, S. Arias-Herrera, and A. Martínez-González, *J Clin Exp Dent* 13, 520 (2021).
11. S. Sarfraz, P.H. Mäntynen, M. Laurila, S. Rossi, J. Leikola, M. Kaakinen, J. Suojanen, and J. Reunanen, *Polymers (Basel).* 14, 52 (2022).
12. S. Ali, O.A. Aziz, and M. Ahmed, *Maxillofac Plast. Reconstr. Surg.* 44, 52 (2022).
13. B. Kasemo, *Surf. Sci.* 500, 656 (2002).
14. R. Pemmada, V.S. Telang, P. Tandon, and V. Thomas, *J. Mech. Behav. Biomed. Mater.* 151, 106397 (2024).
15. C. Karthik, S. Rajalakshmi, S. Thomas, and V. Thomas, *Curr. Opin. Biomed. Eng.* 26, 100440 (2023).
16. R.R. Pillai, K. Appavoo, C.T. Lungu, S.K. Behura, and V. Thomas, *ACS Appl. Polym. Mater.* 2, 96 (2023).
17. G. Amokrane, C. Falentin-Daudré, S. Ramtani, and V. Migonney, *Irbm* 39, 268 (2018).
18. G. Amokrane, V. Humblot, E. Jubeli, N. Yagoubi, S. Ramtani, V. Migonney, and C. Falentin-Daudré, *ACS Omega* 4, 17194 (2019).
19. R. Zaplotnik, and A. Vesel, *Polymers (Basel).* 12, 69 (2020).
20. B. Oriented, 1 (2023).
21. L. Pérez-Álvarez, L. Ruiz-Rubio, I. Moreno, and J.L. Vilas-Vilela, *Polymers (Basel).* 11, 1 (2019).
22. J.P. Bradford, B. Tucker, G. Hernandez-Moreno, P. Charles, and V. Thomas, *J. Mater. Sci.* 56, 14717 (2021).
23. B. Pidhatika, V.T. Widyaya, P.C. Nalam, Y.A. Swasono, and R. Ardhani, *Polymers (Basel).* 14, 1 (2022).
24. C. Zimmerer, M. Schwind, S. Putzke, R. Frenzel, A. Drechsler, and F. Simon, *J. Adhes. Sci. Technol.* 38, 139 (2024).
25. D. Yu, X. Lei, and H. Zhu, *J. Zhejiang Univ. Sci. B* 23, 189 (2022).
26. B. Gupta, J.G. Hilborn, I. Bisson, and P. Frey, *J. Appl. Polym. Sci.* 81, 2993 (2001).
27. N. Ninan, B. Joseph, R.M. Visalakshan, R. Bright, C. Denoual, P. Zilm, Y.B. Dalvi, P.V. Priya, A. Mathew, Y. Grohens, N. Kalarikkal, K. Vasilev, and S. Thomas, *Mater. Adv.* 2, 6620 (2021).
28. Y. Chen, Q. Gao, H. Wan, J. Yi, Y. Wei, and P. Liu, *Appl. Surf. Sci.* 265, 452 (2013).
29. S. Yoshida, K. Hagiwara, T. Hasebe, and A. Hotta, *Surf. Coatings Technol.* 233, 99 (2013).
30. A. Cheng, Z. Schwartz, A. Kahn, X. Li, Z. Shao, M. Sun, Y. Ao, B.D. Boyan, and H. Chen, *Tissue Eng. - Part B Rev.* 25, 14 (2019).
31. W. Wang, G. Caetano, W.S. Ambler, J.J. Blaker, M.A. Frade, P. Mandal, C. Diver, and P. Bártolo, *Materials (Basel).* 9, 140 (2016).
32. D. Khanal, J. Kim, J. Zhang, W.R. Ke, M.M.B. Holl, and H.K. Chan, *Int. J. Pharm.* 632, 122563 (2023).
33. S. Solution, and S. Minerals, *J. M. Huggett* 10, 10 (2015).
34. J. Araki, *Cellulose* 28, 7707 (2021).
35. Y. Sasai, A. Komatsu, S.I. Kondo, Y. Yamauchi, and M. Kuzuya, *J. Photopolym. Sci. Technol.* 25, 551 (2012).
36. C. Falentin-Daudré, M. Aitouakli, J.S. Baumann, N. Bouchemal, V. Humblot, V. Migonney, and J. Spadavecchia, *ACS Omega* 5, 8137 (2020).
37. R. Zhang, E. Zhuravlev, R. Androsch, and C. Schick, *Polymers (Basel).* 11, 210 (2019).
38. Y. Wang, B. Chen, K.E. Evans, and O. Ghita, *Mater. Lett.* 184, 112 (2016).
39. Z. Novotna, A. Reznickova, S. Rimpelova, M. Vesely, Z. Kolska, and V. Svorcik, *RSC Adv.* 5, 41428 (2015).
40. A. Sateria, Pristiansyah, and I. Dwisaputra, ICSECC 2020 - 2nd Int. Conf. Sustain. Eng. Creat. Comput. Proc. 164 (2020).
41. Z. Ma, L. Li, X. Shi, Z. Wang, M. Guo, Y. Wang, Z. Jiao, C. Zhang, and P. Zhang, *J. Appl. Polym. Sci.* 137, 1 (2020).
42. Z. Ma, X. Zhao, J. Zhao, Z. Zhao, Q. Wang, and C. Zhang, *Front. Bioeng. Biotechnol.* 8, 1 (2020).

43. Sunarso, A. Tsuchiya, R. Toita, K. Tsuru, and K. Ishikawa, Int. J. Mol. Sci. **21**, 1 (2020).
44. Y. Chen, Y. Feng, J.G. Deveaux, M.A. Masoud, F.S. Chandra, H. Chen, D. Zhang, and L. Feng, *Minerals* 9, 1 (2019).
45. R. Podgórski, M. Wojasiński, and T. Ciach, *Sci. Rep.* 12, 1 (2022).
46. P. Larsson, H. Engqvist, J. Biermann, E. Werner Rönnerman, E. Forssell-Aronsson, A. Kovács, P. Karlsson, K. Helou, and T. Z. Parris, Sci. Rep. **10**, 1 (2020).
47. J. Sims-Mourtada, R.A. Niamat, S. Samuel, C. Eskridge, and E.B. Kmiec, *Int. J. Nanomed.* 9, 995 (2014).